Kinetics of Light-Induced Intramolecular Energy Transfer in Different Conformational States of NADH

*Zsuzsanna Heiner[†§], Thomas Roland[‡], Jérémie Leonard[‡], Stefan Haacke[‡], and Géza I. Groma[†]**

†Institute of Biophysics, Biological Research Centre, Hungarian Academy of Sciences, H-6701 Szeged, Hungary

‡ University of Strasbourg, CNRS, Institut de Physique et Chimie des Matériaux de Strasbourg, UMR7504, F-67000 Strasbourg, France

Corresponding Author

*E-Mail: groma.geza@brc.mta.hu

Present Addresses

§School of Analytical Sciences Adlershof (SALSA), Humboldt University of Berlin, D-12489 Berlin-Adlershof, Germany and Department of Chemistry, Humboldt University of Berlin, D-12489 Berlin-Adlershof, Germany

ABSTRACT

When bound to a protein, the coenzyme NAD+/NADH typically exists in an extended conformation, while in aqueous solutions it can be characterized by an equilibrium of folded and unfolded structures. It was recognized long ago that in the folded conformation light absorption at the adenine ring initiates an effective energy transfer (ET) towards the nicotinamide group, but the mechanism of this process is still unexplored. Here we apply ultrafast transient absorption measurements on NADH combined with compartmental model analysis for following the kinetics of the ET. We find that the actual ET is extremely rapid (~70 fs). The high rate can be well described by a Förster-type mechanism, promoted by both the special photophysical properties of adenine and the sub-nm inter-ring distance. The rapid ET creates a vibrationally hot excited state on nicotinamide, the vibrational and electronic relaxation of which is characterized by 1.7 ps and 650 ps, respectively.

INTRODUCTION

In living cells, the essential coenzyme nicotinamide adenine dinucleotide (NAD) exists in both enzyme-bound and free states. Hierarchical clustering of the enzyme-bound structures of NAD and the related NADP molecules, based on a large set of X-ray data, resulted in 11 distinct clusters[1]. The majority of these structures correspond to unfolded conformations in which the distance separating the C^{6A} of the adenine (A) and the C^{2N} of the (dihydro)nicotinamide (NA) groups is larger than 12 Å. Due to the lack of X-ray data for the free states, the conformations of the oxidized (NAD^+) or reduced (NADH, Scheme 1) state of the coenzyme in solutions can be explored only by indirect methods. The results of extensive studies involving NMR[2-5], absorption[6], fluorescence[7-13], circular dichroism[14] and IR[5] spectroscopy together with molecular dynamics calculations[15] can be summarized in a model describing a dynamic equilibrium between folded and unfolded states with a relatively high fraction of the former one in aqueous solutions. Nevertheless, this model is not free of contradictions, especially in the interpretation of the fluorescence kinetics data on direct excitation at NA. In contrast to its counterpart coenzyme flavin adenine dinucleotide (FAD), showing an expected shorter fluorescence lifetime in its folded conformation,[16] NAD^+/NADH have shorter lifetimes in their unfolded states.[10-11, 13] This unusual order is explained by exciplex formation between the A and NA rings in the folded conformation.[10] However, still there is no direct proof for this interpretation of the biexponential fluorescence decay of NA[17]. Alternative models suppose a reversible excited-state reaction,[18] other (unspecified) photoprocesses[19] or need to explain even more complex kinetics.[20-21] The situation calls for a detailed investigation of the excited state processes of NADH. The question of structural heterogeneity is best addressed by femtosecond spectroscopy,[22-23] when carried out as a function of the ratio of folded to unfolded species.

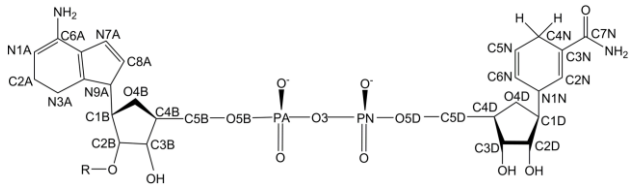

Scheme 1. The chemical structure of NADH

The close interaction between the two rings of NADH in its folded conformation is also indicated by the effective excited-state ET manifested in an intensive fluorescence from NA when the molecule is excited at A.[7-9, 12, 24-25] The explanation of the ET mechanism must be carried out in the light of the numerous studies reported on the special photoprocesses taking place on different model molecules for isolated A, as the 9H tautomer of adenine (9H-Ade) and its 9H-substituted analogues adenosine (Ado) and 2'-deoxyadenosine-5'-monophosphate (dAMP).[26] Time-resolved absorption,[27-31] fluorescence[30-33] and photoelectron[34] spectroscopy data indicate that the excited states of these molecules depopulate non-radiatively in an extremely rapid (≤100-300 fs) process, thus setting a narrow sub-picosecond time window that makes efficient ET in NADH challenging.

Surprisingly, the photoprocesses of NADH have been scarcely studied by the methods of modern femtosecond time-resolved spectroscopy.[5] Transient absorption (TA) experiments carried out with ps/ns time resolution by exciting at NA could not explore the details of the excited-state events, and mainly focus on the photoproducts such as ionic and radical forms of NADH and solvated electrons.[35-38] To our knowledge, no similar study has been performed so far involving excitation of A. To fill these gaps here we show that applying TA measurement of high time resolution on aqueous solutions of NADH in which the equilibrium of the folded and unfolded conformers was controlled by the presence of methanol (MeOH),[2, 6, 8, 12, 39] it is possible to obtain a detailed map on the successive steps of the ET process from the excited A donor to the NA acceptor.

EXPERIMENTAL METHODS

Materials

β-NADH was purchased from Sigma-Aldrich in the form of disodium salt hydrate and was dissolved, without further purification, in 0.1 M PIPES (piperazine-N,N′-bis(2-ethanesulfonic acid)) buffer at pH 7.0. PIPES was proven to provide better conditions for cofactors than phosphate buffer due to the higher coenzyme degradation in the latter[40]. 3×10^{-4} M NADH solution in the different mixture of the buffer and MeOH was prepared freshly and was kept at 24 ˚C during the TA measurements.

Steady-state spectra

The absorption spectra of NADH (Figure S1A) were recorded with a spectrophotometer before and after each TA measurement to monitor the optical density and chemical stability of the solutions. The change in the absorption spectra was negligible during the course of the measurements.

For estimating the efficiency of the ET the excitation spectra detected at 470 nm and corrected for instrument response (Figure S1B) and the emission spectra excited at 266 nm (Figure S1C) were also detected at different MeOH concentrations [MeOH].

TA measurements

The apparatus for TA measurement was previously described in detail.[41] Briefly, the beam of an amplified Ti:Sapphire system (5 kHz, 40 fs, 500 μJ) was split into two parts. One of them generated third harmonic pulses at 266 nm, constituting the pump for the sample with optical density of ~0.5, circulating through a 0.5 mm quartz capillary. The other beam travelled through a delay line and

then was focused into a 1.5-mm CaF_2 plate for producing white light continuum (WLC) covering the 330-630-nm spectral range. The WLC beam was then further split into a probe and a reference, both of which passed through a spectrograph and were detected by a cooled CCD camera in order to measure the sample absorbance and the power fluctuation of the WLC, respectively. A chopper on the pump beam allowed recording alternatively the absorption of the sample with and without excitation, from which the differential absorption spectra were computed. The temporal resolution of the apparatus characterized by a wavelength-dependent Gaussian σ parameter described by (S3)-(S7) in Section 1 of the *Supporting Information (SI)* was 60-70 fs. An optimal tradeoff between an adequate signal-to-noise ratio and chemical stability of the samples was found at a pump power of 650 μW. The focal spot diameters of the probe and pump pulses were 35-40 μm and 120 μm, respectively. The relative linear polarization between the pump and probe beams was set at the magic angle (54.7°) to avoid any contribution from the decay of anisotropy.

Analysis of the TA data

All calculations were carried out by homemade programs written in MATLAB.

First the raw data went through a preprocessing procedure described in Section 1 of the *SI* for removing the artifacts due to occasional bubbling in the sample and executing chirp correction and noise filtering. After that the datasets obtained for each [MeOH] were analyzed by a least-square fitting procedure, supposing exponential decay of two or three components. The actual fitting functions were constructed by the convolution described in (S4). In the first step of the analysis the kinetics at six characteristic wavelengths were fitted independently. The results of this model are shown in Figure S2 and Table S1. The final presented results were obtained by a more sophisticated

global fitting model in which for a given sample the time constants of the exponentials were global free parameters while the amplitudes at every wavelength were local ones.

The above models took into account the corruption of the true TA signal – corresponding to pure NADH – by the contribution of the solvent, mainly due to creation of solvated electrons by excitation of water.[42] This error was corrected by subtracting the signal measured on the same mixture of PIPES buffer and MeOH in the absence of NADH, multiplied by a weighting factor lying in the (0, 1) interval. The proper value of this factor (in the first approximation independent of [MeOH]) was determined in two different ways. In the first approach, the weighting factors were also free parameters of the above fitting model, and then the obtained values were averaged. In the second one, the fittings were calculated with fixed weighting factor values from the sequence of 0.2, 0.3, ..., 0.8, and the results were visually inspected for minimizing the features in the residuals. Both methods indicated that 0.5 is the optimal weighting factor.

RESULTS AND DISCUSSION

The occurrence of the ET process upon excitation at the A group is illustrated by the existence of the band around 260 nm in the steady-state excitation spectrum of NADH (Figure 1A). For the corresponding absorption and emission spectra see Figure S1 of the *Supporting Information (SI)*. In full consistency with previous findings,[12] the relative weight of this band decreases by adding MeOH which shifts the equilibrium of NADH conformers toward the unfolded states. Let us suppose that the ET takes place only from the excited state of NADH molecules being in the folded conformation and the probability of this process is p. Then denoting the fraction of this conformation at a given [MeOH] by f, an effective efficiency of the process can be calculated from the peak ratios in the absorption and excitation spectra, denoted A and E respectively, as (see Section 2 of the *SI* for details):

$$\eta \equiv fp = \frac{E_{260}A_{340}}{E_{340}A_{260}} \quad (1)$$

The dependence of this effective efficiency on [MeOH], taking into account the contribution of NA to the absorbance at 250 nm[9, 43] is presented in Figure 1B.

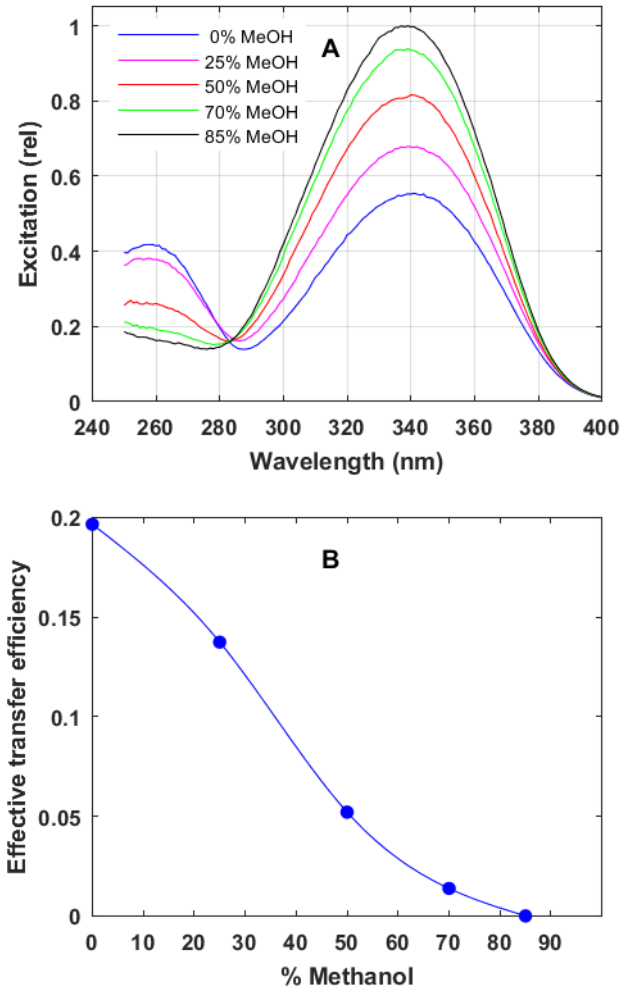

Figure 1. (A) Steady-state fluorescence excitation spectrum of NADH in different MeOH:water mixtures detected at 470 nm (B) Effective transfer efficiency calculated from (1) (see Section 2 of the *SI* for the details)

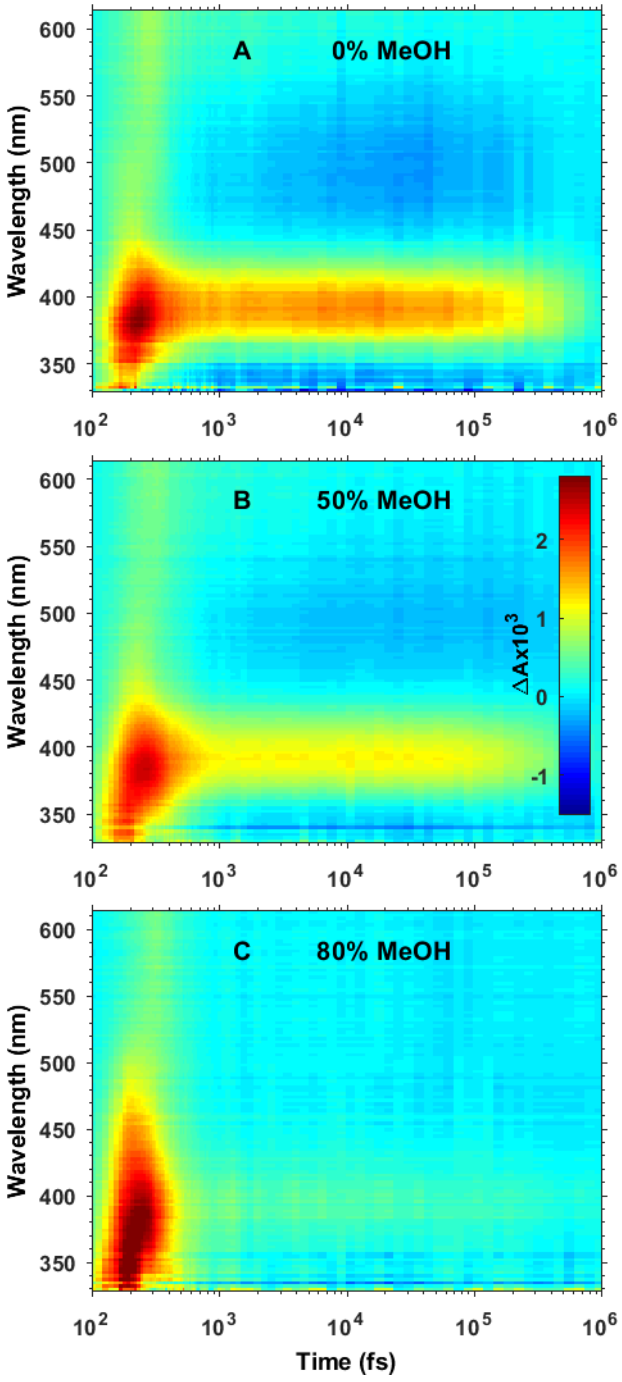

Figure 2. Temporal and spectral distribution of the light-induced absorption change of NADH in (A) 0%, (B) 50% and (C) 80% MeOH:water. The pump pulse had a spectral peak at 266 nm. Red and blue colors indicate positive and negative absorbance change, respectively.

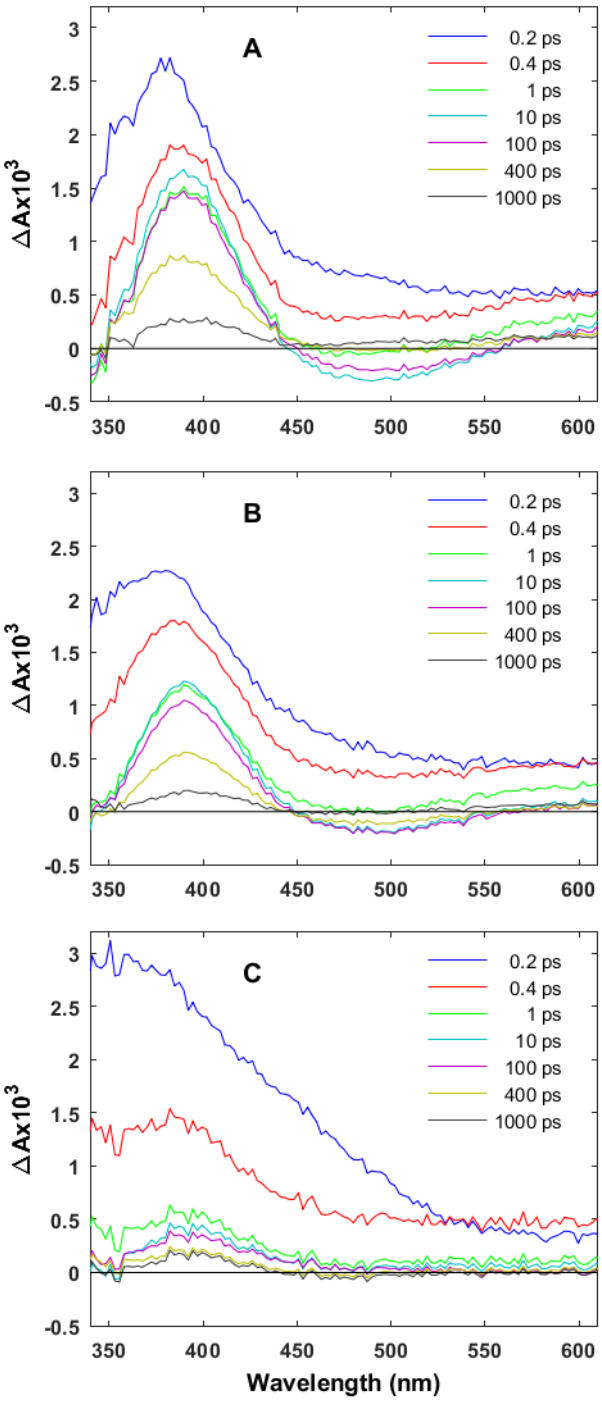

Figure 3. Time evolution of the TA spectra of NADH in (A) 0%, (B) 50% and (C) 80% MeOH:water after the pump pulse.

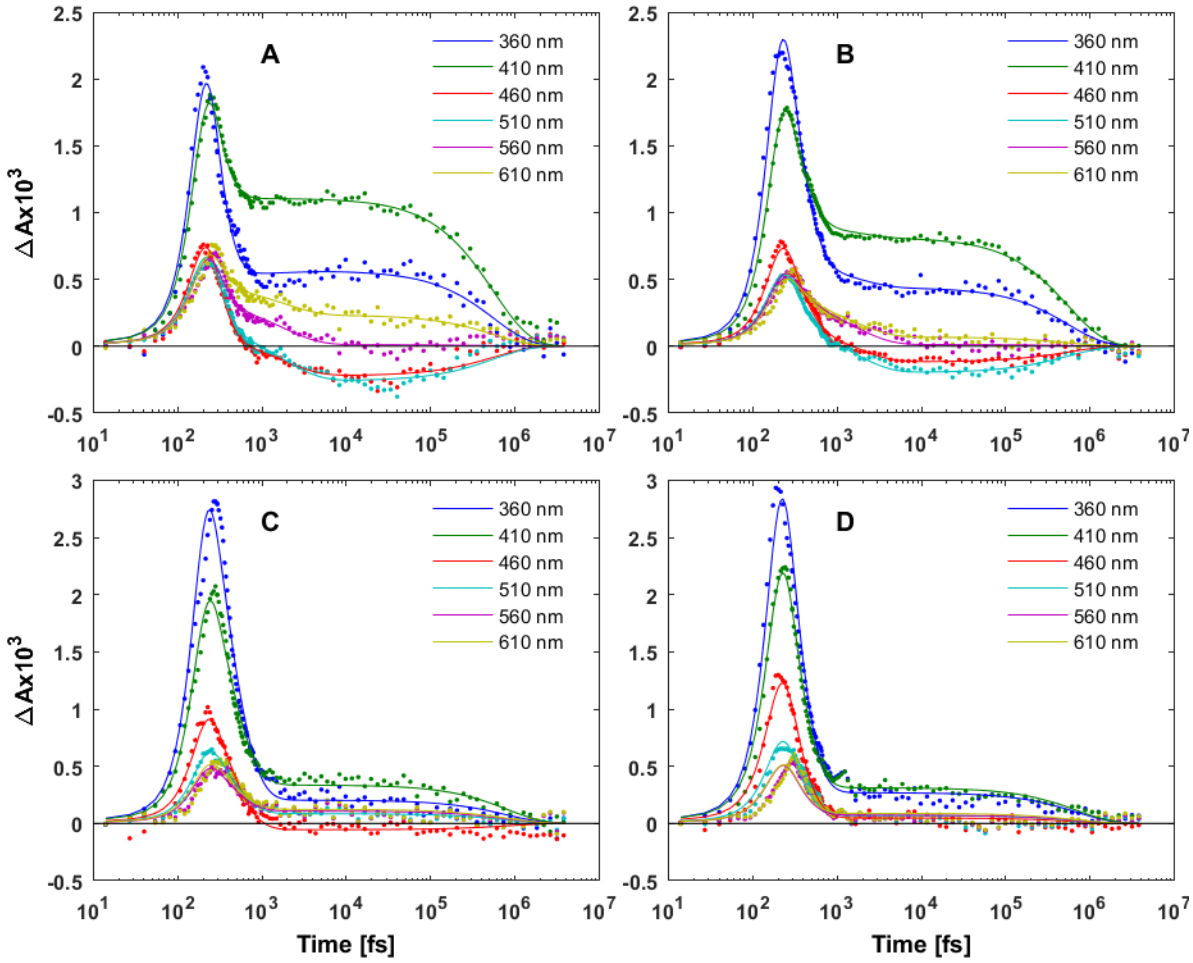

Figure 4. Dotted line: TA kinetics of NADH in (A) 0%, (B) 50%, (C) 70% and (D) 80% MeOH:water at different wavelengths in response to the pump pulse. Solid lines: result of the global fitting by the applied kinetic model (see the text and the SI).

The overall temporal and spectral distribution of the TA signal of NADH excited in the absorption band of A (266 nm) is shown in Figure 2 for different values of [MeOH]. The most striking feature are two long-lived components, that dim out for higher [MeOH], one absorbing at ~390 nm and a weaker negative band at ~500 nm. The latter is dominated by the stimulated emission (SE) of NA, as indicated by the good agreement with the shape of the steady-state fluorescence spectrum of NA (Figure S1C). With increasing [MeOH], the fraction of the molecules

in folded states and the effective ET efficiencies are reduced[8, 12] (Figure S2), leading to reduced amplitudes of the long-lived SE and the induced, most likely excited state absorption (ESA) of NA at 390 nm. The details of this process illustrated by the temporal evolution of the TA spectra (Figure 3) and the kinetic traces at representative wavelengths (Figure 4, dotted lines), however, indicate more complex features, such as an ultrafast red-shift and decay of the near-UV ESA and a slower progressive change in the kinetics (cf. traces at 460 and 510 nm) in the first picoseconds.

It is obvious to suppose that an adequate model for the experimental TA kinetics can be based on a set of first order reactions, since only intra-molecular processes are involved. Accordingly, as a first step, the TA dataset was analyzed by individually fitting the kinetics at a few wavelength values with a sum of exponentials, as presented in Figure S3 and Table S1. In the absence of MeOH the kinetics can be characterized by three components with well-separated time constants of ~150 fs, 0.5-8 ps and 0.5-0.8 ns. Although fluctuating in value, the intermediate picosecond component is clearly present in the raw data, in particular for pure H_2O, but the kinetics for [MeOH]> 50% are well fitted without it. The 0.5-0.8 ns value of the third time constant coincides well with that reported for the lifetime of fluorescence originating from direct excitation of NA[9-11, 13, 19-21]. Based on this coincidence, the spectral similarity discussed above and the fact that its weight markedly decreases at increasing [MeOH], this component can be clearly assigned to the excited-state lifetime of NA.

In order to retrieve the reaction scenario, in a second stage of the analysis the datasets were projected onto decay associated difference spectra (DADS),[44] allowing to model them with a relatively small number of kinetic parameters by applying a global fitting method. The fitting curves obtained are plotted as solid lines in Figure 4 and the corresponding DADS are presented in Figure 5. This somewhat simplified model still describes all important features of the experimental traces with a good overall accuracy. In addition, the resulting time constants (Table 1) characterize

the kinetics at every [MeOH] with definitely low deviations. Obviously, with the measuring device characterized by a Gaussian IRF of σ = 60-70 fs, the fastest component is properly resolved, with typically +/- 50 fs error bar.

Table 1. Time constants obtained from the global fitting of the kinetics.

	0% MeOH	50% MeOH	70% MeOH	80% MeOH
τ_1 (fs)	120 ± 38[a]	180 ± 90	280 ± 70	170 ± 12
τ_2 (ps)	1.8 ± 0.9	1.6 ± 1.4	-	-
τ_3 (ns)	0.56 ± 0.48	0.55 ± 0.15	0.80 ± 0.71	0.69 ± 0.25

[a]See Section 5 of the *SI* for the detailed description of uncertainty estimation applied to the parameters in this table and the text.

Since τ_3 is assigned to the excited-state lifetime of NA populated by the ET, the transfer process itself has to occur either with τ_1 or τ_2 or both. The important conclusion here is that the kinetics of the ET hardly depends on [MeOH], which rather has an influence on the amplitudes of the DADS (Figure 5). This suggests that the presence of MeOH does not increase the distance between N and A, which would result in a progressive increase of the ET time. The observations are best described by the co-existence of open and closed forms, with an equilibrium population favoring the open configuration at higher [MeOH]. This model is in agreement with the previous results on fluorescence ET studies.[8, 12]

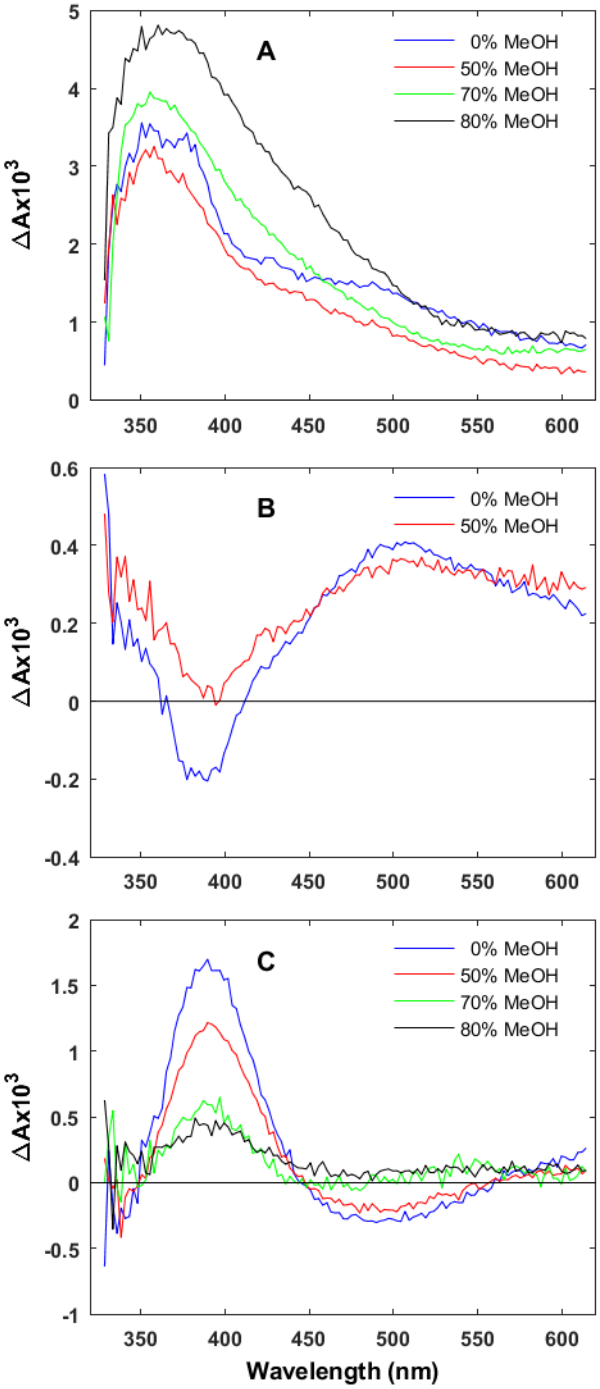

Figure 5. Decay associated difference spectra (DADS) of NADH corresponding to the apparent time constants (A) τ_1, (B) τ_2 and (C) τ_3 presented in Table 1 (see the text and the SI for the detailed kinetic model). The τ_2 component does not take place in the kinetics at 70% and 80% methanol content.

In the final step of the analysis we have to derive the three experimental DADSs from a particular compartmental model, characterized by microscopic rate constants.[44] The simplest model is a sequence of first order reactions involving three transient components T_j, the last of which returns to the initial ground state R, with zero differential absorption:

$$T_1 \xrightarrow{k_1} T_2 \xrightarrow{k_2} T_3 \xrightarrow{k_3} R \tag{2}$$

According to the derivation[45] outlined in Section 3 of the *SI*, the corresponding set of DADS are

$$\begin{aligned} D_1(\lambda) &= \varepsilon_1(\lambda) + \frac{k_1}{k_2 - k_1}\varepsilon_2(\lambda) + \frac{k_1 k_2}{(k_2 - k_1)(k_3 - k_1)}\varepsilon_3(\lambda) \\ D_2(\lambda) &= \frac{k_1}{k_1 - k_2}\varepsilon_2(\lambda) + \frac{k_1 k_2}{(k_1 - k_2)(k_3 - k_2)}\varepsilon_3(\lambda) \\ D_3(\lambda) &= \frac{k_1 k_2}{(k_1 - k_3)(k_2 - k_3)}\varepsilon_3(\lambda) \end{aligned} \tag{3}$$

where $\varepsilon_j(\lambda)$ is the extinction coefficient of state *j* at wavelength λ. Since in (2) T_j generally cannot be assigned to a single chemical compound, $\varepsilon_j(\lambda)$ is the signed sum of the extinction coefficients of all compounds contributing to that state. A negative value of $\varepsilon_j(\lambda)$ means that either bleaching or SE dominates in state *j*.

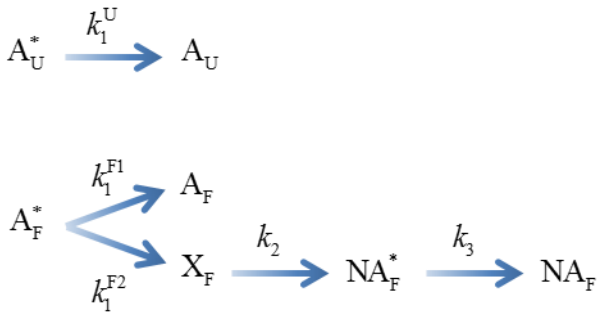

Scheme 2. The proposed kinetic model of NADH photoreactions.

The actual model of NADH photoreactions in water:MeOH mixtures requires parallel sequences of events as summarized in Scheme 2, since both open and closed forms of NADH coexist. Here index U and F denote the unfolded and folded conformation of the NADH molecules, respectively, and asterisks indicate electronically excited states. NA_F^* denotes the vibrationally relaxed excited state of NA that generates the steady-state fluorescence or the long-lived SE. In the first approximation the rate constants in the scheme do not depend on [MeOH], which has effect only on the fraction *f* of NADH molecules in the folded state. It was supposed that in the unfolded molecules the excited A group simply returns to its ground state, without ET, as represented on the uppermost transition in the scheme. It is expected that a fraction of the folded molecules also relax by this way, which corresponds to the higher branch of the events originating from A_F^*. The lower branch, describing the ET process is also efficiently operative, leading to the observed longer-lived excited state of NA.

Since the time resolution and noise level of our measurements did not make possible to decompose the femtosecond components belonging to the folded and unfolded fraction of the molecules, the measured value of τ_1 can be considered as a weighted average approximated by

$$\frac{1}{\tau_1} = (1 - f)\,k_1^{U} + f\left(k_1^{F1} + k_1^{F2}\right) \qquad (4)$$

With the plausible hypothesis that $k_1^{U} \approx k_1^{F1}$ (4) predicts an increase of τ_1 with increasing [MeOH] (i.e. decreasing f), and a slight but significant tendency in this direction is truly observable in Table 1. Sorting the conformational states of NADH to native (0% MeOH) and denatured (70% and 80% MeOH) categories, the corresponding average lifetimes are $\tau_1^{n} = 120 \pm 38$ fs and $\tau_1^{d} = 230 \pm 36$ fs, assigned to the fractions f^{n} and f^{d}, respectively. The value of f^{d} calculated from steady-state

spectra is practically zero (Figure 1B). These simplifications result in $k_1^{U} = \frac{1}{\tau_1^{d}}$, excellently in accordance with the excited-state lifetime (≤100-300 fs) reported for 9H-Ade, Ado and dAMP.[26-34] Since the probability of the ET can be expressed by the rate constants as $p = \frac{k_1^{F2}}{k_1^{F1} + k_1^{F2}}$ (4) yields

$$1 + \frac{f^{n} p}{1 - p} = \frac{\tau_1^{d}}{\tau_1^{n}} = 1.9 \qquad (5)$$

With $f^{n} p = 0.2$ as indicated in Figure 1B one obtains $p = 0.77 \pm 0.17$, in accordance with the observed efficient ET. Consequently, for pure water $f = 0.26 \pm 0.06$, falling in the range of 0.24-0.35 obtained from NMR[3-4] and fluorescence lifetime[11] measurements. Most importantly, the calculated rate constant of the ET is $k_1^{F2} = (1.5 \pm 1.4) \times 10^{13}\ \mathrm{s}^{-1}$, which is higher by two orders of magnitude than estimated in an early study.[9] The corresponding time constant is $\tau_{ET} = 67 \pm 62$ fs.

As a consequence of the above assignment of τ_1, in the lowest reaction route k_2 and k_3 are assigned to $\tau_2 = 1.7 \pm 0.8$ ps and $\tau_3 = 650 \pm 230$ ps, respectively (averaged values in Table 1). In this route the transient states presented in (2) can be identified as follows. In the T_1 state A_F is bleached and A_F^* is populated, hence the corresponding extinction coefficient is

$$\varepsilon_1(\lambda) = \varepsilon_{A_F^*}(\lambda) - \varepsilon_{A_F}(\lambda) \qquad (6)$$

In T_2 A_F^* is transformed to a yet unspecified X_F state and A_F is still bleached, that is

$$\varepsilon_2(\lambda) = \varepsilon_{X_F}(\lambda) - \varepsilon_{A_F}(\lambda) \qquad (7)$$

Finally, T_3 corresponds to a state where the ET is concluded in parallel processes: in this state both the population of X_F and the bleaching of A_F have disappeared, in parallel NA_F is turned into its excited state, consequently its ground state is bleached. This implies

$$\varepsilon_3(\lambda) = \varepsilon_{NA_F^*}(\lambda) - \varepsilon_{NA_F}(\lambda) \tag{8}$$

With the above assignment of the rate constants and transient states, ignoring the contribution of k_1^{F1} and substituting (6), (7) and (8) into (3), the ET route (2) becomes

$$\begin{aligned} D_1(\lambda) &= \varepsilon_{A_F^*}(\lambda) + 0.03\varepsilon_{A_F}(\lambda) - 1.03\varepsilon_{X_F}(\lambda) + 0.03\left[\varepsilon_{NA_F^*}(\lambda) - \varepsilon_{NA_F}(\lambda)\right] \\ D_2(\lambda) &= 1.03\left[\varepsilon_{X_F}(\lambda) - \varepsilon_{A_F}(\lambda)\right] - 1.03\left[\varepsilon_{NA_F^*}(\lambda) - \varepsilon_{NA_F}(\lambda)\right] \\ D_3(\lambda) &= 1.00\left[\varepsilon_{NA_F^*}(\lambda) - \varepsilon_{NA_F}(\lambda)\right] \end{aligned} \tag{9}$$

As discussed above and described by (4) the two higher reaction routes in Scheme 2 also have contribution to τ_1 and – supposing spectral identity in them – the corresponding DADS is

$$D_1(\lambda) = \varepsilon_1(\lambda) = \varepsilon_{A_U^*}(\lambda) - \varepsilon_{A_U}(\lambda) \tag{10}$$

which becomes practically exclusive in 70% or 80% MeOH. According to (9), in the presence of ET the two major components contributing to $D_1(\lambda)$ are A_F^* and X_F with positive and negative signs, respectively. In the absence of that (10) indicates that $D_1(\lambda)$ is the difference spectra of A_U^* and A_U, the absorption spectrum of the latter is out of the observed spectral range. Considering the corresponding experimental spectrum (Figure 5A) it consists of a main positive peak at ~360 nm, the shape of which is identical at every [MeOH]. This means that this peak is attributable to the ESA corresponding to both A_F^* and A_U^*, the spectra of which are truly indistinguishable. This

interpretation is consistent with the high amplitude of this peak as compared to the two other experimental DADS (panel B and C in Figure 5) which can be assigned exclusively to the ET route (see below). A close peak at ~380 nm was also observed in the ESA of both Ado[30] and dAMP,[31] supporting this assignment. However, the additional weak peak around 600 nm occurring in the ESA of these model compounds is missing in this DADS at any [MeOH], indicating that even in the open conformer of NADH the electronic band system of A in some extent is perturbed by NA. In pure water an additional feature of negative band at ~400 nm and a positive one at ~500 is added to the main peak. Both the size and the shape of this feature is similar to that in panel B and C of Figure 4, showing mirror symmetry to each other. Since the contribution of X_F is largest in pure water, this additional pair of bands is attributed to this component (see also below).

The second experimental DADS (Figure 5B) can be easily interpreted as the difference spectrum of NA_F and NA_F^*, according to the second term of $D_2(\lambda)$ in (9). Indeed, the positive peak at the low wavelength edge corresponds to the absorption of NA_F, having maximum at 340 nm (Figure S1A). In harmony with the interpretation of the features in Figure 2, the negative peak at ~390 nm is attributed to ESA of NA_F^*, while the second positive band peaking at ~510 nm to the SE of that, both with inverted signs since the population of NA_F^* is rising. This interpretation is in accordance with the fact that the second component of the kinetics disappears at high [MeOH], where the efficiency of the ET vanishes. The first term of $D_2(\lambda)$ in (9) has no significant or apparent contribution to the experimentally obtained DADS. This is expected for the ground state bleach of A_F, the absorption band of which is located <300 nm. To explain the contribution of X_F we have to suppose that it is spectrally indistinguishable from NA_F^*. Indeed, since the ET occurs on a <100 fs timescale, it resonantly populates NA_F^* at higher vibrational levels, meaning that X_F is a

vibrationally excited form of NA_F^*. Then, vibrational cooling, typically occurring on a time scale of a few ps, explains the rate constant k_2, and the spectrum of X_F is very akin to the one of NA_F^*, in agreement with the observations, however with an expected spectral narrowing going unnoticed. A process of vibrational cooling taking place on a similar time scale following the rapid deactivation of the excited state was also reported from TA studies on Ado[27-28, 30] as well as from fluorescence kinetic experiments exciting NADH at either its A or NA group,[25] supporting this interpretation. In $D_2(\lambda)$ the spectra of X_F and NA_F^* take place in different sign. This is consistent with the low amplitude observable in Figure 5B, the sign of which indicates that the spectrum of NA_F^* is the dominating one. Also this interpretation is in harmony with our assignment of the extra feature appearing in Figure 5A in the absence of MeOH to X_F.

The third experimental DADS (Figure 5C) is due to the excited state decay of NA_F^*, as indicated by the expression for $D_3(\lambda)$ in (9), in accordance with the explained good coincidence of τ_3 with the lifetime values available in the literature. The almost perfect mirror symmetry of the experimental difference spectra with that in Figure 5B is in line with the dominance of the second term related to NA_F^* in $D_2(\lambda)$, which strengthens the above interpretations. Moreover, this DADS also highly reduces with increasing [MeOH] as expected from our model. Note that, in contrast to the observation of different photoproducts on direct excitation of the NA group[35-38], no indication of their occurrence was found when in our experiments NA_F^* was populated by ET. Nevertheless, unlike the second component, the third DADS does not completely vanish at 70-80% MeOH where the effective efficiency of the ET is very low (Figure 1B). This might be explained by a small amount of direct excitation of NA via its extended absorption at 260 nm.[9, 43]

Regarding the unusually high rate of the ET, it is consistent with the well-known Förster-type ET formalism,[46] which expressed with our notation states that

$$\frac{1}{\tau_{ET}} = \frac{1}{\tau_1^d}\left(\frac{R_0}{r}\right)^6 \tag{11}$$

This means that in this formalism τ_{ET} is inherently scaled by τ_1^d (the excited-state lifetime of the donor in the absence of the acceptor) which is very low itself (230 fs). Knowing the donor-acceptor distance *r* and the Förster radius R_0 – calculable from steady-state spectroscopic data and an orientation factor κ^2 according to (S20) – the probability of ET can be independently determined also from the Förster model in the form of

$$p_F = \frac{R_0^6}{R_0^6 + r^6} \tag{12}$$

A value of r = 0.52 nm can be estimated from the average inter-ring distance calculated in a molecular dynamics study on NAD+ in explicit water.[15] Although this study reports also an average value of 148° for the angle between the two groups together with other structural parameters, to obtain an established value for κ^2 more direct calculations of the transition dipole moment orientations would be needed. In the absence of this, R_0 and p_F were calculated for the whole interval of [0, 4] where the possible values of κ^2 fall in,[46] applying the fluorescence spectrum and quantum yield of dAMP[47] as a model for the A group (see Section 4 of the *SI* for the details). As shown in Figure 6 the obtained Förster radius is very low, mainly due to the low (6.8×10^{-5}) quantum yield of A, as a consequence of its ultrafast nonradiative relaxation. However, it is still higher than inter-ring distance unless κ^2 is considerably lower than 2/3, the value corresponding to the random mutual orientation of the donor and acceptor transition moment. Accordingly, in a very wide range

of κ^2 the probability p_F lies within the one standard deviation band of p, calculated from the kinetic data. This robust coincidence indicates that – despite the extremely low distance between the donor and the acceptor, the Förster theory, elaborated for very weak coupling, describes accurately the high efficiency of the ET, and also confirms the self-consistency of our model.

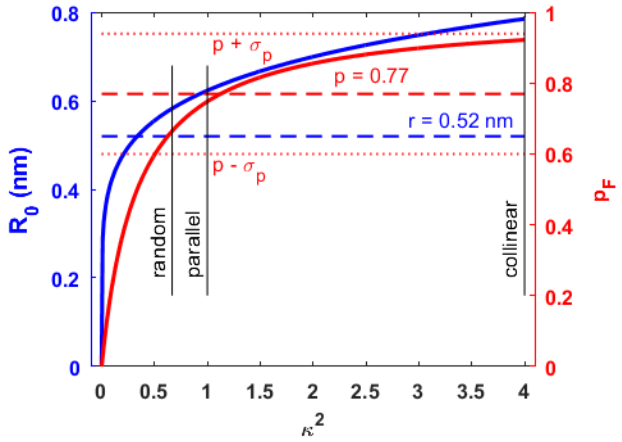

Figure 6. The Förster radius R_0 and the corresponding probability of the energy transfer p_F calculated with inter-ring distance of $r = 0.52$ nm along the whole interval of the orientation factor κ^2. For comparison the mean value of the probability $p = 0.77$ calculated from the kinetic data together with its band of one standard deviation are also presented. The vertical lines mark the values of κ^2 at special mutual orientations of the donor and acceptor transition moments.

The above findings, however, do not exclude alternative models for the ET process. According to an interesting early idea, the occurrence of the longer (0.69 ns) component in the fluorescence decay of NADH can be explained by exciplex formation between the two rings.[10] This model is based on the direct excitation of NA and supposes exciplex formation in the ns timescale, hence in its original form is incompatible with our findings. Nonetheless, one can suppose that an ultrafast

exciplex formation can be initiated on excitation of the A group. Indeed, theoretical studies on the adenine analogue 2-aminopurine, forming π-stacking interactions with adenine or guanine nucleobases resulted in the occurrence of minima on the potential energy surfaces, corresponding to exciplex formation.[48] Transient absorption and time-resolved fluorescence experiments on adenine dinucleotides[49] and $(dA)_{20}$ oligonucleotide[30] indicate light-induced formation of excimer states of lifetimes orders of magnitude higher than that of the localized excited state characteristic to the monomers.[30, 49] The underlying energy transfer process leading to a collective excited state was also explained by stacking interactions. Similar long-lived components were observed on double helix poly(dA)·poly(dT) samples, explained by the development of a collective excited state in the frame of exciton theory, not supposing exciplex formation, but excluding Förster-type energy transfer.[50] Note that the DADSs observed in our study do not provide indications of excimer-related emission, but are consistent with the above minimal reaction scenario. In addition, π-stacking, governing the collective excited states is unlikely in NADH since the conjugation in the NA group is disrupted by reduction. Nevertheless, some form of charge translocation upon the ET cannot be excluded. Clearly, detailed and dedicated future studies are necessary to shed more light on the exact nature of this extremely fast process.

CONCLUSIONS

The main focus of this study is to kinetically characterize the sequence of the events initiated by the excitation of the NADH molecule at its A group. We find that for the fraction of molecules in folded conformation ($f = 0.26$) the actual energy transfer is completed in a very rapid (~70 fs) step, taking place with a probability of $p = 0.77$. The sudden acceptance of energy creates a vibrationally hot excited state of NA, and the corresponding vibrational cooling takes place in the second step (1.7 ps). Finally, the excited NA relaxes to its ground state (650 ps).

In addition to the above kinetic description we made an attempt to disclose also the mechanism of the ET process. Formal application of the Förster-type dipole-dipole interaction model resulted in a surprisingly good agreement in the probability (and hence inherently also in the rate) of the ET with the value obtained by the above kinetic analysis. No indications in our data were found supporting the occurrence of collective excited states in the form of an exciplex or exciton, which would be possible alternatives of a true Förster mechanism and were proven to have substantial role in the photoprocesses of adenine di- and oligonucleotides. On the other hand, the actual ET could be more complex than that dictated by the Förster model, the validity of which is indeed questionable for the present sub-nm donor-acceptor distances. It was found, however, that in many cases where the orbital overlap of the two chromophores has be also taken into account to properly describe the ET process, the Förster model still provides good approximations since the dipole-dipole interaction remains the dominant Coulombic component.[46]

SUPPORTING INFORMATION AVAILABLE

1. Pre-processing of TA data 2. Derivation of the energy transfer efficiency from the steady-state spectra 3. Derivation of the kinetic model 4. Calculation of the Förster radius 5. Uncertainty estimation of the calculated parameters 6. Additional figures and tables. The Supporting Information is available free of charge on the ACS Publications website at DOI:

CORRESPONDING AUTHOR

*Email: groma.geza@brc.mta.hu

NOTES

The authors declare no competing financial interests.

ACKNOWLEDGMENT

This work was supported by the National Research, Development and Innovation Office of Hungary under grant GINOP-2.3.2-15-2016-00001 and co-financed by the European Regional Fund. The Strasbourg group acknowledges technical assistance from O. Crégut.

REFERENCES

1. Kuppuraj, G.; Sargsyan, K.; Hua, Y. H.; Merrill, A. R.; Lim, C. Linking distinct conformations of nicotinamide adenine dinucleotide with protein fold/function. *J. Phys. Chem. B* **2011,** *115* (24), 7932-7939.

2. Catterall, W. A.; Hollis, D. P.; Walter, C. F. Nuclear magnetic resonance study of the confirmation of nicotinamide-adenine dinucleotide and reduced nicotinamide-adenine dinucleotide insolution. *Biochemistry* **1969,** *8* (10), 4032-4036.

3. Oppenheimer, N. J.; Arnold, L. J.; Kaplan, N. O. A structure of pyridine nucleotides in solution. *Proc. Natl. Acad. Sci. U. S. A.* **1971,** *68* (12), 3200-3205.

4. McDonald, G.; Brown, B.; Hollis, D.; Walter, C. Effects of environment on the folding of nicotinamide-adenine dinucleotides in aqueous solutions. *Biochemistry* **1972,** *11* (10), 1920-1930.

5. Simpson, N.; Shaw, D. J.; Frederix, P. W. J. M.; Gillies, A. H.; Adamczyk, K.; Greetham, G. M.; Towrie, M.; Parker, A. W.; Hoskisson, P. A.; Hunt, N. T. Infrared spectroscopy of nicotinamide adenine dinucleotides in one and two dimensions. *J. Phys. Chem. B* **2013,** *117* (51), 16468-16478.

6. Cross, D. G.; Fisher, H. F. Conformation and conformational changes of reduced diphosphopyridine nucleotide in solution. *Biochemistry* **1969,** *8* (3), 1147-1155.

7. Weber, G. Intramolecular transfer of electronic energy in dihydro diphosphopyridine nucleotide. *Nature* **1957,** *180* (4599), 1409-1409.

8. Freed, S.; Neyfakh, E. A.; Tumerman, L. A. Influence of solvents on the intramolecular energy transfer in NADH and NADPH. *Biochim. Biophys. Acta* **1967,** *143* (2), 432-434.

9. Scott, T. G.; Spencer, R. D.; Leonard, N. J.; Weber, G. Synthetic spectroscopic models related to coenzymes and base pairs. V. Emission properties of NADH. Studies of fluorescence lifetimes and quantum efficiencies of NADH, AcPyADH, and simplified synthetic models. *J. Am. Chem. Soc.* **1970,** *92* (3), 687-695.

10. Visser, A. J. W. G.; van Hoek, A. The fluorescence decay of reduced nicotinamides in aqueous-solution after excitation with a UV-mode locked Ar ion laser. *Photochem. Photobiol.* **1981,** *33* (1), 35-40.

11. Couprie, M. E.; Merola, F.; Tauc, P.; Garzella, D.; Delboulbe, A.; Hara, T.; Billardon, M. First use of the UV super-ACO free-electron laser: Fluorescence decays and rotational-dynamics of the NADH coenzyme. *Rev. Sci. Instrum.* **1994,** *65* (5), 1485-1495.

12. Hull, R. V.; Conger, P. S.; Hoobler, R. J. Conformation of NADH studied by fluorescence excitation transfer spectroscopy. *Biophys. Chem.* **2001,** *90* (1), 9-16.

13. Vishwasrao, H. D.; Heikal, A. A.; Kasischke, K. A.; Webb, W. W. Conformational dependence of intracellular NADH on metabolic state revealed by associated fluorescence anisotropy. *J. Biol. Chem.* **2005,** *280* (26), 25119-25126.

14. Miles, D. W.; Urry, D. W. Reciprocal relations and proximity of bases in pyridine dinucleotides. *J. Biol. Chem.* **1968,** *243* (16), 4181-4188.

15. Smith, P. E. Molecular dynamics simulations of NAD+ in solution. *J. Am. Chem. Soc.* **1999,** *121* (37), 8637-8644.

16. Chosrowjan, H.; Taniguchi, S.; Mataga, N.; Tanaka, F.; Visser, A. J. W. G. The stacked flavin adenine dinucleotide conformation in water is fluorescent on picosecond timescale. *Chem. Phys. Lett.* **2003,** *378* (3-4), 354-358.

17. Blacker, T. S.; Marsh, R. J.; Duchen, M. R.; Bain, A. J. Activated barrier crossing dynamics in the non-radiative decay of NADH and NADPH. *Chem. Phys.* **2013,** *422* (0), 184-194.

18. Gafni, A.; Brand, L. Fluorescence decay studies of reduced nicotinamide adenine dinucleotide in solution and bound to liver alcohol dehydrogenase. *Biochemistry* **1976,** *15* (15), 3165-3171.

19. Krishnamoorthy, G.; Periasamy, N.; Venkataraman, B. On the origin of heterogeneity of fluorescence decay kinetics of reduced nicotinamide adenine dinucleotide. *Biochem. Biophys. Res. Commun.* **1987,** *144* (1), 387-392.

20. Ladokhin, A. S.; Brand, L. Evidence for an excited-state reaction contributing to NADH fluorescence. *Journal of Fluorescence* **1995,** *5* (1), 99-106.

21. Nakabayashi, T.; Islam, M. S.; Li, L.; Yasuda, M.; Ohta, N. Studies on external electric field effects on absorption and fluorescence spectra of NADH. *Chem. Phys. Lett.* **2014,** *595*, 25-30.

22. Voltz, K.; Leonard, J.; Touceda, P. T.; Conyard, J.; Chaker, Z.; Dejaegere, A.; Godet, J.; Mely, Y.; Haacke, S.; Stote, R. H. Quantitative sampling of conformational heterogeneity of a DNA hairpin using molecular dynamics simulations and ultrafast fluorescence spectroscopy. *Nucleic Acids Res.* **2016,** *44* (7), 3408-3419.

23. Groma, G. I.; Heiner, Z.; Makai, A.; Sarlos, F. Estimation of kinetic parameters from time-resolved fluorescence data: A compressed sensing approach. *RSC Adv.* **2012,** *2* (30), 11481-11490.

24. Spencer, R. D.; Weber, G. Measurements of subnanosecond fluorescence lifetimes with a cross-correlation phase fluorometer. *Ann. N. Y. Acad. Sci.* **1969,** *158* (1), 361-376.

25. Ho, Y. F. Femtosecond broadband time-resolved fluorescence and transient absorption investigation on the excited states of model DNA oligomers containing adenine. PhD Thesis, The Hong Kong Polytechnic University, Hong Kong, 2014.

26. Crespo-Hernandez, C. E.; Cohen, B.; Hare, P. M.; Kohler, B. Ultrafast excited-state dynamics in nucleic acids. *Chem. Rev.* **2004,** *104* (4), 1977-2019.

27. Pecourt, J. M. L.; Peon, J.; Kohler, B. Ultrafast internal conversion of electronically excited RNA and DNA nucleosides in water. *J. Am. Chem. Soc.* **2000,** *122* (38), 9348-9349.

28. Pecourt, J. M. L.; Peon, J.; Kohler, B. DNA excited-state dynamics: Ultrafast internal conversion and vibrational cooling in a series of nucleosides. *J. Am. Chem. Soc.* **2001,** *123* (42), 10370-10378.

29. Cohen, B.; Hare, P. M.; Kohler, B. Ultrafast excited-state dynamics of adenine and monomethylated adenines in solution: Implications for the nonradiative decay mechanism. *J. Am. Chem. Soc.* **2003,** *125* (44), 13594-13601.

30. Kwok, W.-M.; Ma, C.; Phillips, D. L. Femtosecond time- and wavelength-resolved fluorescence and absorption spectroscopic study of the excited states of adenosine and an adenine oligomer. *J. Am. Chem. Soc.* **2006,** *128* (36), 11894-11905.

31. Stuhldreier, M. C.; Temps, F. Ultrafast photo-initiated molecular quantum dynamics in the DNA dinucleotide d(ApG) revealed by broadband transient absorption spectroscopy. *Faraday Discuss.* **2013,** *163*, 173-188.

32. Gustavsson, T.; Sharonov, A.; Onidas, D.; Markovitsi, D. Adenine, deoxyadenosine and deoxyadenosine 5 '-monophosphate studied by femtosecond fluorescence upconversion spectroscopy. *Chem. Phys. Lett.* **2002,** *356* (1-2), 49-54.

33. Pancur, T.; Schwalb, N. K.; Renth, F.; Temps, F. Femtosecond fluorescence up-conversion spectroscopy of adenine and adenosine: experimental evidence for the πσ* state? *Chem. Phys.* **2005,** *313* (1), 199-212.

34. Buchner, F.; Ritze, H.-H.; Lahl, J.; Lübcke, A. Time-resolved photoelectron spectroscopy of adenine and adenosine in aqueous solution. *Phys. Chem. Chem. Phys.* **2013**.

35. Boldridge, D. W.; Morton, T. H.; Scott, G. W. Formation kinetics and quantum yield of photon-induced electron ejection from NADH in aqueous solution. *Chem. Phys. Lett.* **1984,** *108* (5), 461-465.

36. Lindqvist, L.; Czochralska, B.; Grigorov, I. Determination of the mechanism of photo-ionization of NADH in aqueous-solution on laser excitation at 355 nm. *Chem. Phys. Lett.* **1985,** *119* (6), 494-498.

37. Pakalnis, S.; Sitas, V.; Schneckenburger, H.; Rotomskis, R. Picosecond absorption spectroscopy of biologically active pigments NADH, FMN and fluorescence marker rhodamine-123. http://www.photobiology.com/photobiology2000/VSitas/ps_abs_sp_index.htm (accessed July 21, 2017).

38. Takahashi, N.; Shinno, T.; Tachikawa, M.; Yuzawa, T.; Takahashi, H. Time-resolved resonance Raman, time-resolved UV-visible absorption and DFT calculation study on photo-oxidation of the reduced form of nicotinamide adenine dinucleotide. *J. Raman Spectrosc.* **2006,** *37* (1-3), 283-290.

39. Tropp, J.; Redfield, A. G. Proton magnetic resonance of NADH in water-methanol mixtures. Conformational change and behavior of exchangeable proton resonances as a function of temperature. *J. Am. Chem. Soc.* **1980,** *102* (2), 534-538.

40. Rover, L.; Fernandes, J. C. B.; Neto, G. D.; Kubota, L. T.; Katekawa, E.; Serrano, S. H. P. Study of NADH stability using ultraviolet-visible spectrophotometric analysis and factorial design. *Anal. Biochem.* **1998,** *260* (1), 50-55.

41. Sinicropi, A.; Martin, E.; Ryazantsev, M.; Helbing, J.; Briand, J.; Sharma, D.; Leonard, J.; Haackee, S.; Cannizzo, A.; Chergui, M., et al. An artificial molecular switch that mimics the visual pigment and completes its photocycle in picoseconds. *Proc. Natl. Acad. Sci. U. S. A.* **2008,** *105* (46), 17642-17647.

42. Assel, M.; Laenen, R.; Laubereau, A. Retrapping and solvation dynamics after femtosecond UV excitation of the solvated electron in water. *J. Chem. Phys.* **1999,** *111* (15), 6869-6874.

43. Weber, G. Transfert d'énergie dans la dihydro-diphosphopyridine nucléotide. *J. Chim. Phys. Phys.-Chim. Biol.* **1958,** *55* (11-12), 878-886.

44. van Stokkum, I. H. M.; Larsen, D. S.; van Grondelle, R. Global and target analysis of time-resolved spectra. *Biochim. Biophys. Acta* **2004,** *1657* (2-3), 82-104.

45. Nagle, J. F.; Parodi, L. A.; Lozier, R. H. Procedure for testing kinetic-models of the photocycle of bacteriorhodopsin. *Biophys. J.* **1982,** *38* (2), 161-174.

46. Valeur, B.; Berberan-Santos, M. N. Molecular fluorescence: Principles and applications. Second ed.; Wiley-VHC: Weinheim, Germany, 2013; pp 213-261.

47. Onidas, D.; Markovitsi, D.; Marguet, S.; Sharonov, A.; Gustavsson, T. Fluorescence properties of DNA nucleosides and nucleotides: A refined steady-state and femtosecond investigation. *J. Phys. Chem. B* **2002,** *106* (43), 11367-11374.

48. Liang, J.; Nguyen, Q. L.; Matsika, S. Exciplexes and conical intersections lead to fluorescence quenching in π-stacked dimers of 2-aminopurine with natural purine nucleobases. *Photochemical & Photobiological Sciences* **2013,** *12* (8), 1387-1400.

49. Chen, J.; Kohler, B. Base stacking in adenosine dimers revealed by femtosecond transient absorption spectroscopy. *J. Am. Chem. Soc.* **2014,** *136* (17), 6362-6372.

50. Markovitsi, D.; Onidas, D.; Gustavsson, T.; Talbot, F.; Lazzarotto, E. Collective behavior of Franck−Condon excited states and energy transfer in DNA double helices. *J. Am. Chem. Soc.* **2005,** *127* (49), 17130-17131.

TOC GRAPHICS

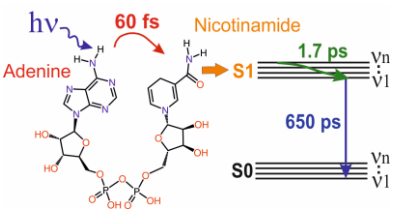

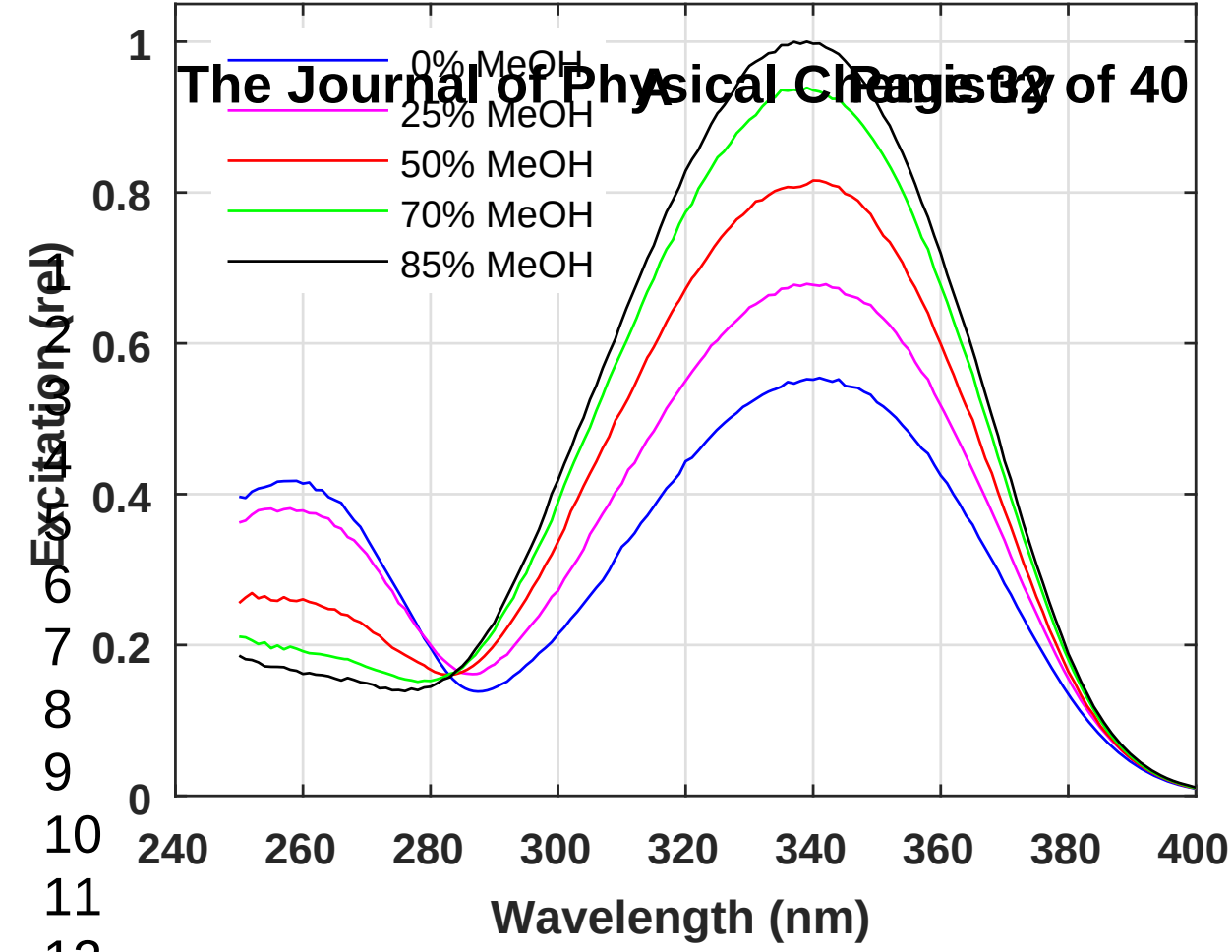
0% MeOH
25% MeOH
50% MeOH
70% MeOH
85% MeOH
Excitation (rel)
Wavelength (nm)
0
0.2
0.4
0.6
0.8
1
240
260
280
300
320
340
360
380
400

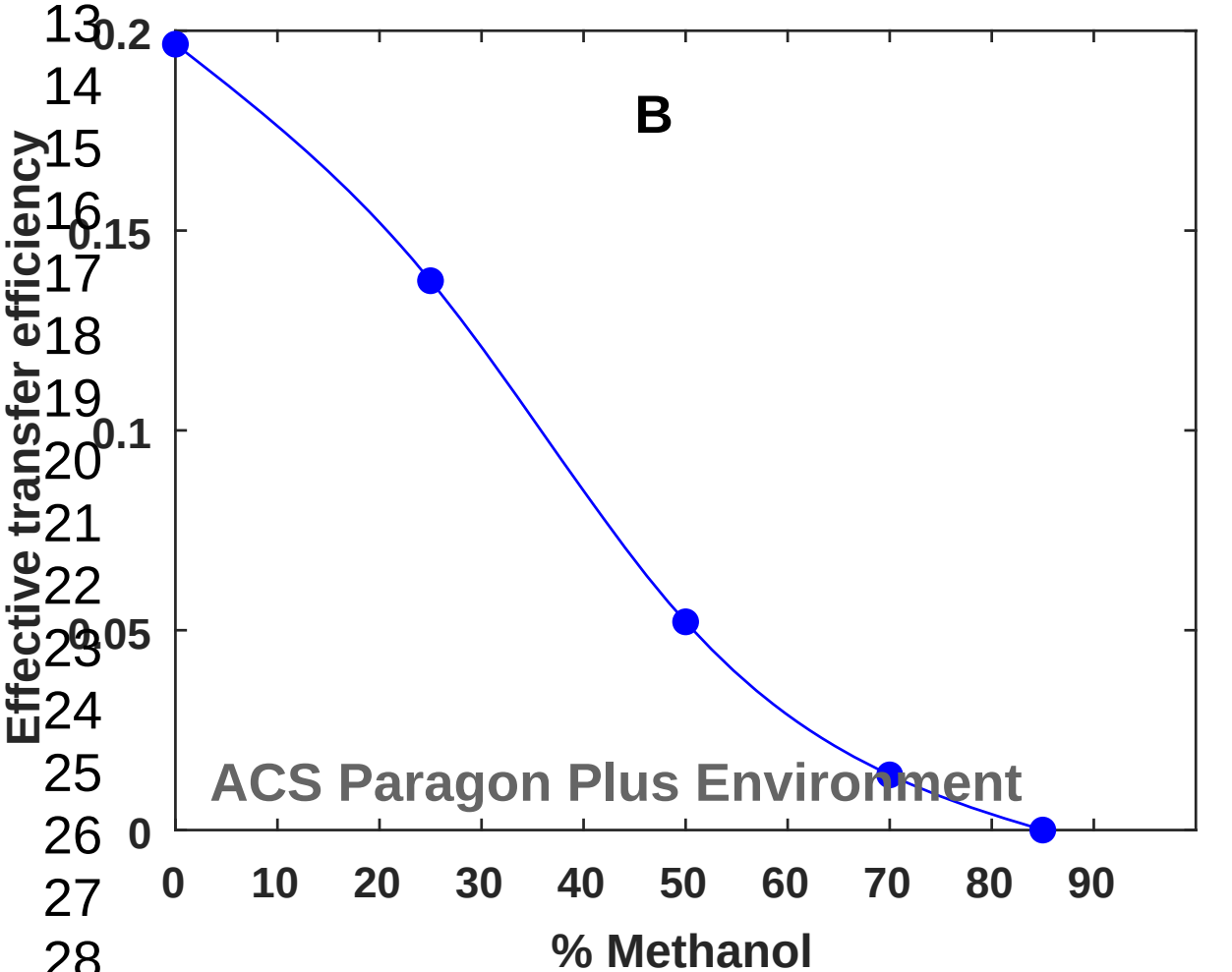
B
Effective transfer efficiency
% Methanol
ACS Paragon Plus Environment
0
0.05
0.1
0.15
0.2
0
10
20
30
40
50
60
70
80
90

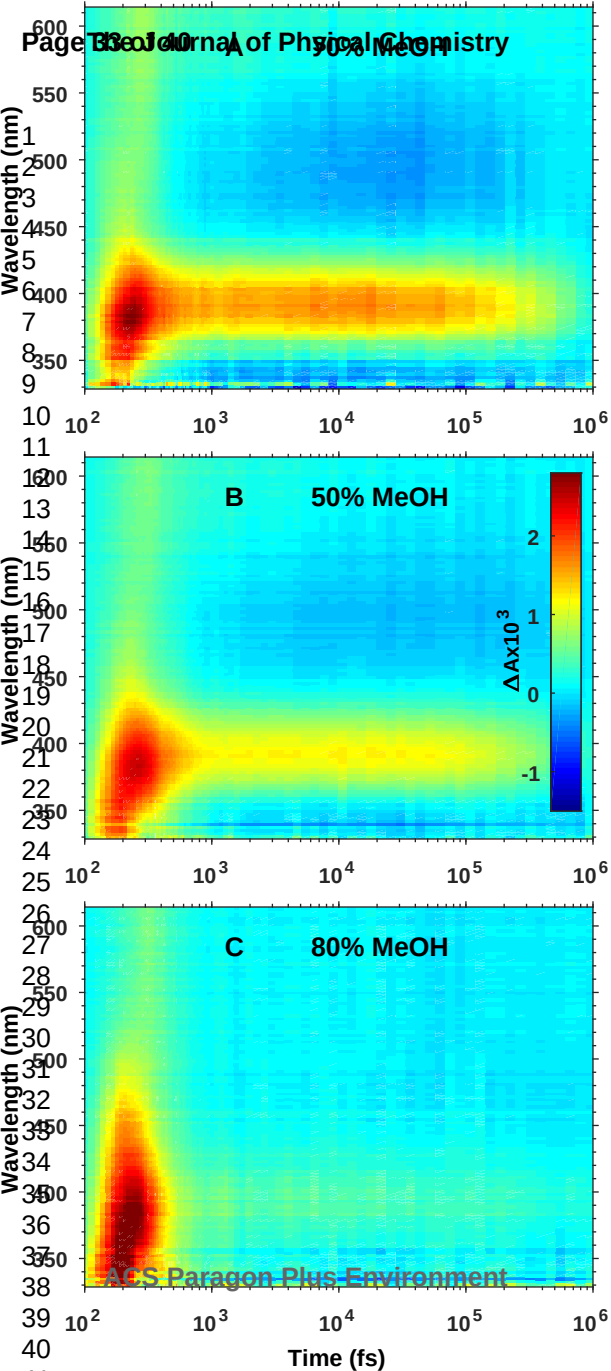

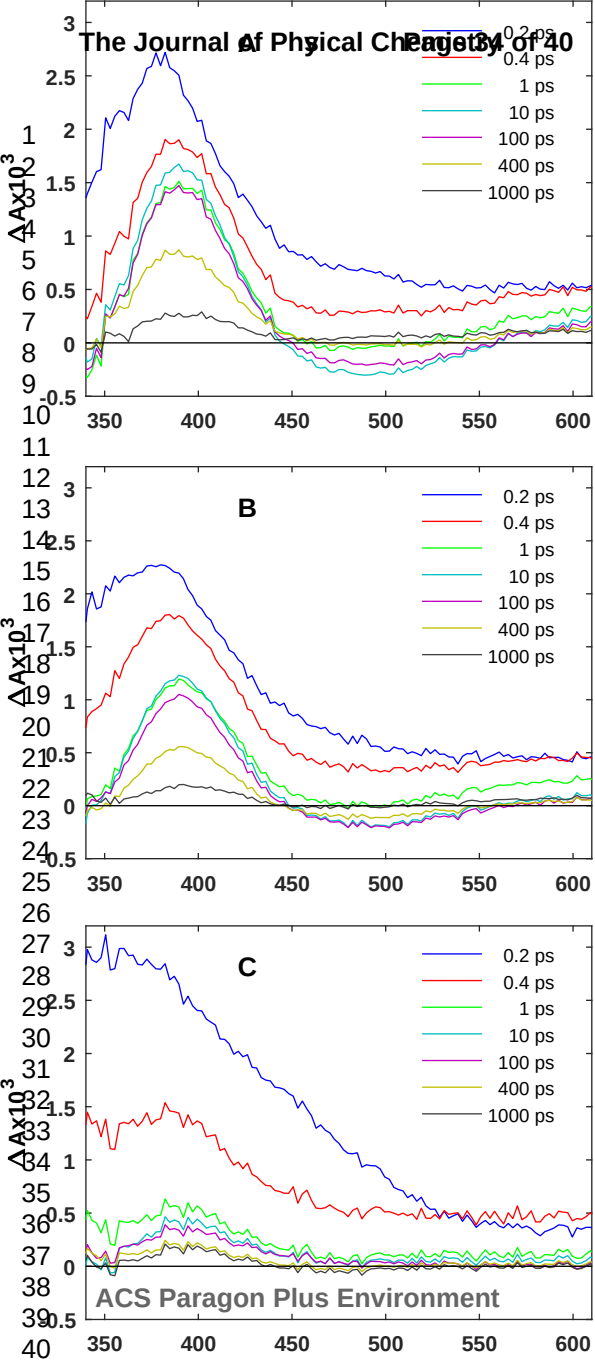
A
B
C
0.2 ps
0.4 ps
1 ps
10 ps
100 ps
400 ps
1000 ps
ΔAx10^3
Wavelength (nm)
ACS Paragon Plus Environment

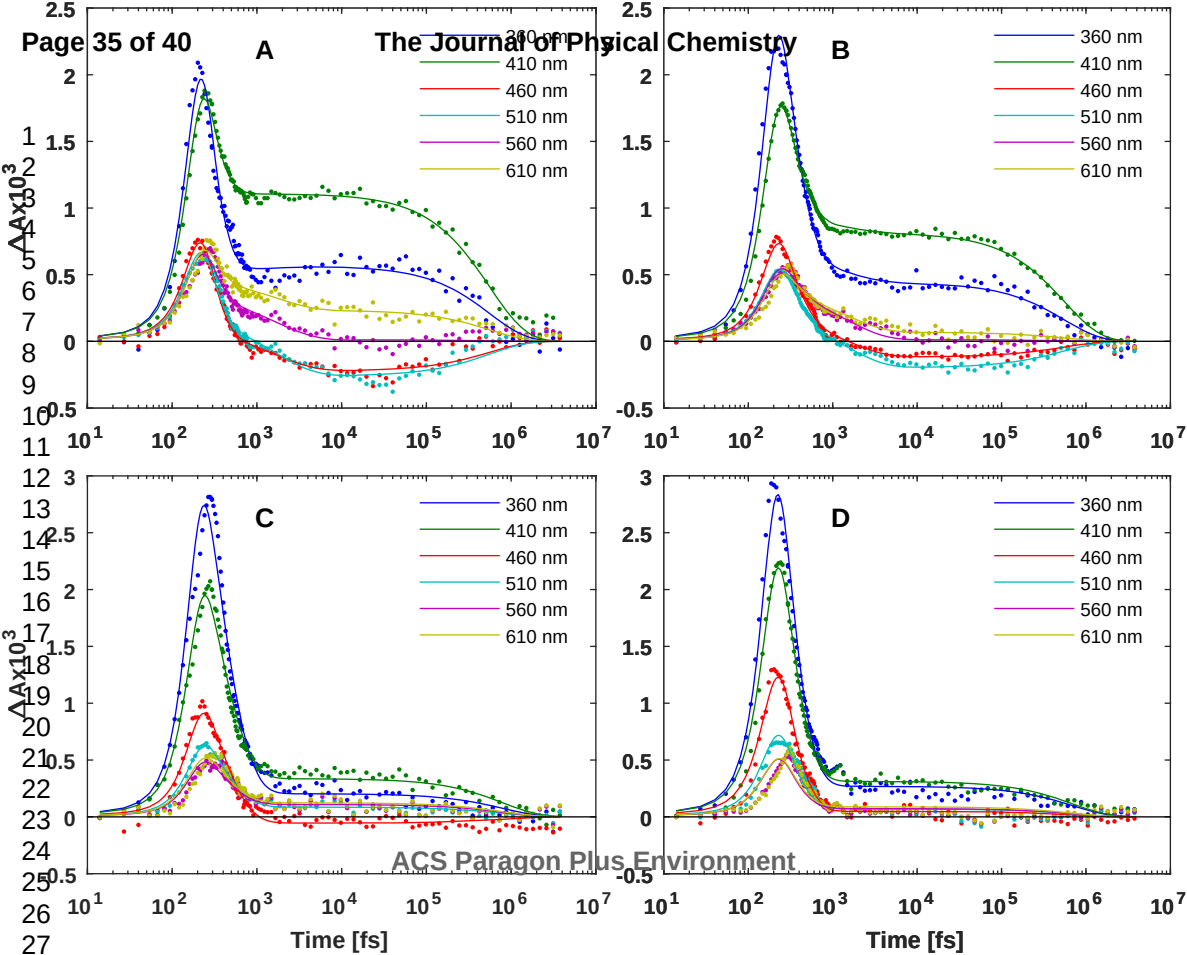

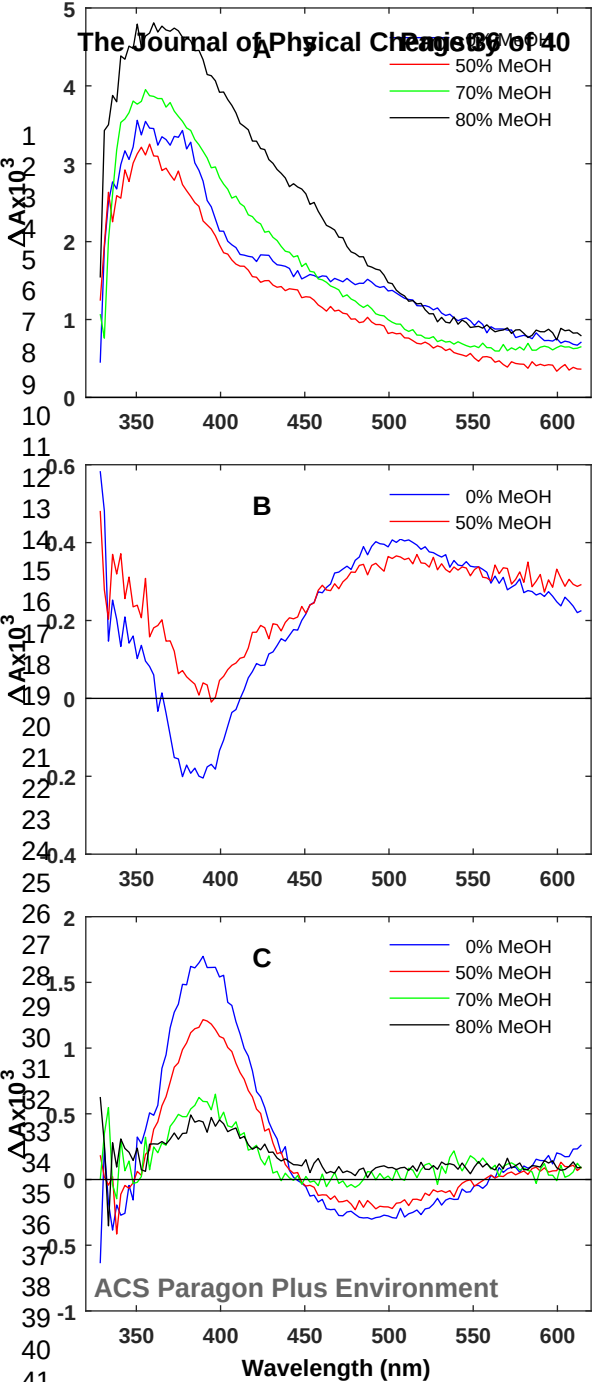
A
50% MeOH
70% MeOH
80% MeOH
ΔAx10^3
B
0% MeOH
50% MeOH
ΔAx10^3
C
0% MeOH
50% MeOH
70% MeOH
80% MeOH
ΔAx10^3
ACS Paragon Plus Environment
Wavelength (nm)

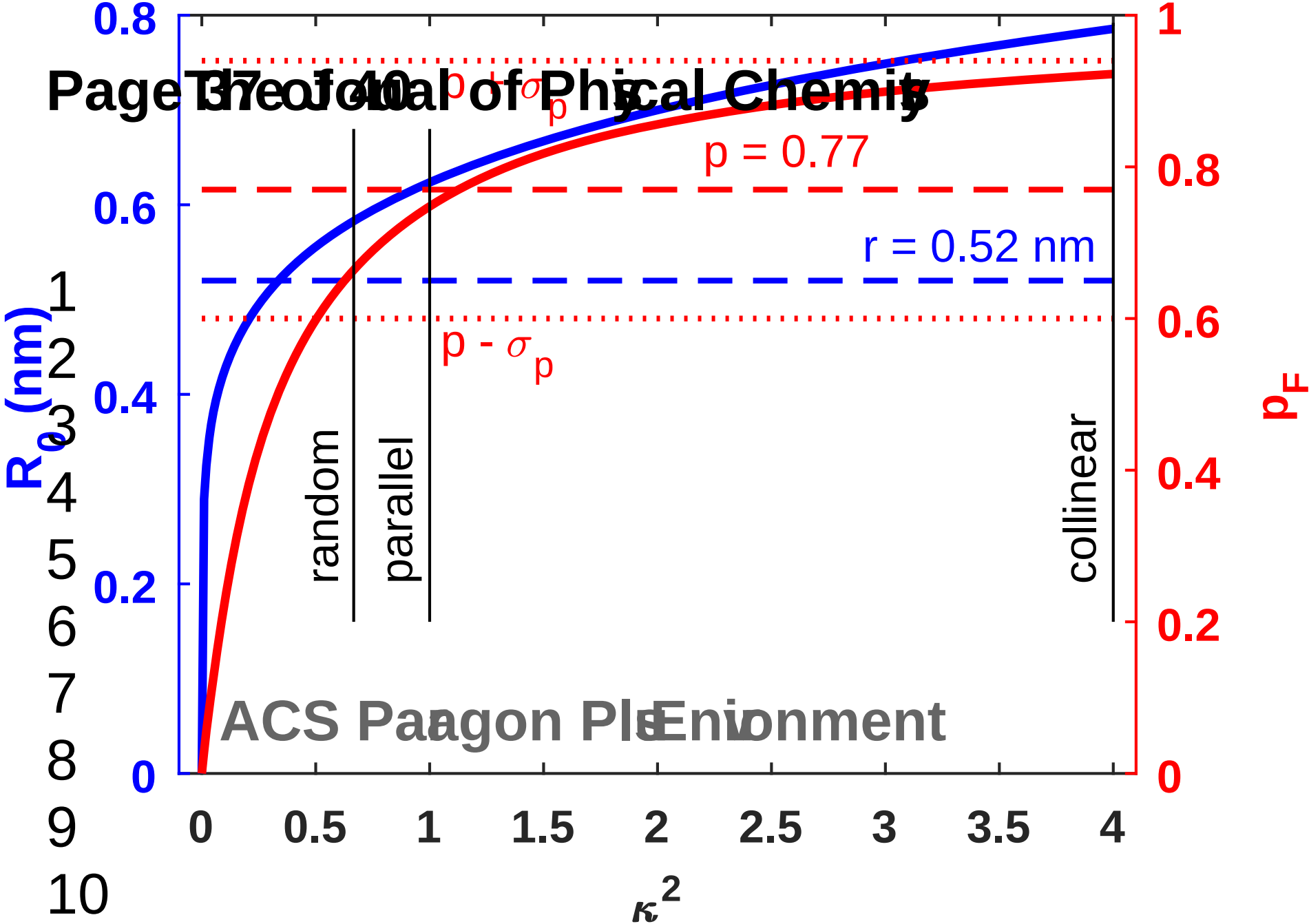

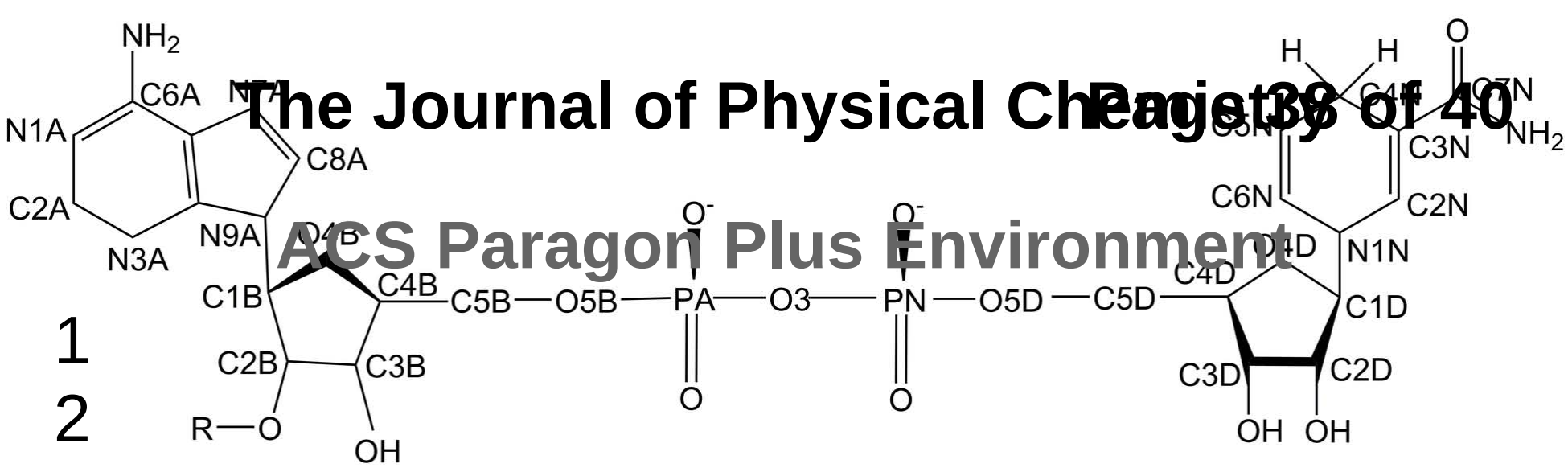

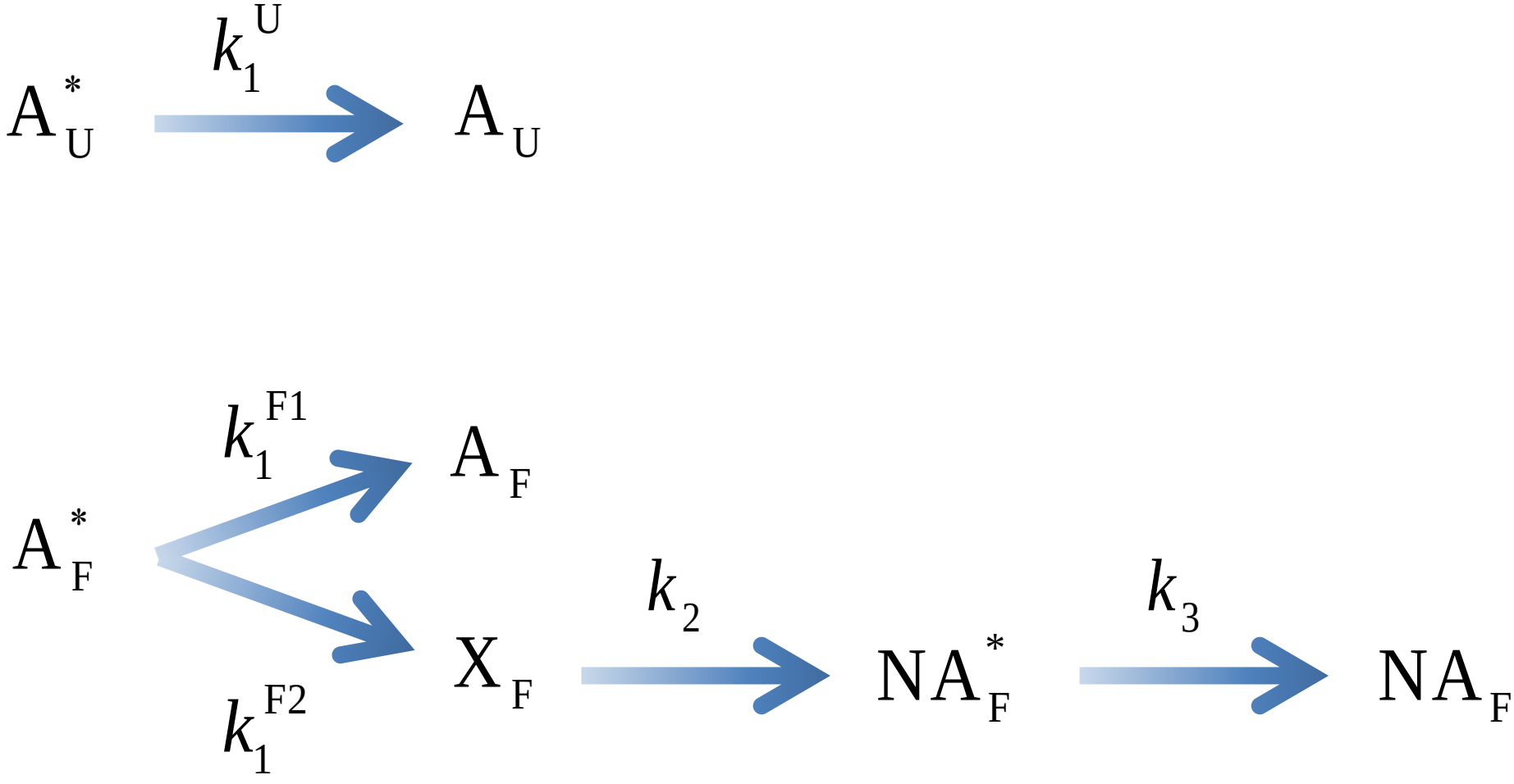
A^*_U
k_1^U
A_U
A^*_F
k_1^{F1}
A_F
k_1^{F2}
X_F
k_2
NA^*_F
k_3
NA_F